Available online at www.sciencedirect.com
ScienceDirect
Geochimica et Cosmochimica Acta 71 (2007) 1281–1289
Geochimica
www.elsevier.com/locate/gca

Equilibrium interface segregation in the diopside–forsterite system II: Applications of interface enrichment to mantle geochemistry

Takehiko Hiraga [a,b,*], Marc M. Hirschmann [a], David L. Kohlstedt [a]

[a] Department of Geology and Geophysics, University of Minnesota, Minneapolis, MN 55455, USA
[b] Earthquake Research Institute, University of Tokyo, 1-1-1 Yayoi, Bunkyo-ku, Tokyo 113-0032, Japan

Received 12 July 2006; accepted in revised form 13 November 2006

Abstract

Segregation of incompatible elements at grain interfaces may have considerable influence on the physical and chemical properties of mantle rocks. Using a recently developed predictive model to estimate the interface enrichment of elements based on their mineral/melt partitioning (Hiraga and Kohlstedt, companion paper), we consider interface enrichment for a simplified model peridotite consisting of olivine, orthopyroxene, and clinopyroxene. Our calculated results reveal the following: (1) Significant amounts of heavy alkali elements and rare gases likely reside at grain–grain interfaces, whereas interface concentrations of less incompatible are less pronounced. (2) The contribution of the chemical components stored at interfaces to whole-rock chemistry strongly depends on mineral mode and, most importantly, on grain size. (3) Grain size reduction resulting from dynamic recrystallization can increase the total storage of highly incompatible elements on grain interfaces and thereby will diminish their concentration in mineral grains. (4) Analysis of Cs concentrations in mantle clinopyroxenes potentially provides estimates of the grain size of mantle rocks. (5) Transport through peridotite will be dominated by diffusion along interfaces rather than through grain interiors for elements less compatible than Lu.

1. Introduction

Geochemical analyses and modeling generally consider the compositions of minerals and fluids. However, in addition to mineral grains and fluids, rocks also contain planar defects, specifically grain–grain interfaces, including interfaces between grains of the same phase (grain boundaries) and interfaces between unlike phases (interphase boundaries). These interfaces may be significant reservoirs for storage of geochemically important elements (Hiraga et al., 2004). Grain interfaces can be much richer in incompatible elements than the grains themselves, as residence of trace elements in the less restrictive structures of grain interfaces does not produce the large excess strain energies expected for mineral lattices (Hiraga et al., 2004; Hiraga and Kohlstedt, companion paper). The companion paper of Hiraga and Kohlstedt presents experimental results documenting the extent of element segregation on grain–grain interfaces. In the present paper, we use these results to formulate a predictive model for interface segregation for various elements based on the lattice misfit strain theory that has previously been applied to element partitioning between mineral and melt.

To evaluate the extent of interface enrichment, Hiraga and Kohlstedt (companion paper) applied the McLean model (1957), which correlates the equilibrium mole concentration of a solute i (e.g., $i =$ La and Sr) at grain–grain interfaces, $X_i^{\text{interface}}$, with that in grain matrices (i.e., intracrystalline regions), X_i^{GM}, (Hiraga et al., 2004):

$$X_i^{\text{interface}} \approx X_i^{\text{GM}} \cdot \exp\left(\frac{Q_i^{\text{seg}}}{\text{R}T}\right) \tag{1}$$

where RT has the usual meaning. In Eq. (1), Q_i^{seg}, the segregation energy, was approximated by the lattice misfit strain energy:

* Corresponding author.
E-mail address: hirag001@umn.edu (T. Hiraga).

0016-7037/$ - see front matter © 2006 Elsevier Inc. All rights reserved.
doi:10.1016/j.gca.2006.11.020

$$Q_i^{\mathrm{seg}} \approx U_i^{\mathrm{elastic}} = 4\pi E^{\delta} \mathrm{N_A}\left[\frac{r_o}{2}(r_i - r_o)^2 + \frac{1}{3}(r_i - r_o)^3\right] \quad (2)$$

where E^{δ} is the effective Young's modulus of the lattice site, δ, $\mathrm{N_A}$ is Avogadro's number, r_i is the ionic radius of the substitutional cation, and r_o is the optimum radius of the site of interest (for details, see Hiraga and Kohlstedt, companion paper). This approach describes well the segregation behavior of divalent elements. However, to account for the behavior of heterovalent cations in Eq. (2), an electrostatic work term, U_i^{elec}, must be included with U_i^{elastic} in Q_i^{seg} and a revised value for E^{α} must be used for heterovalent ions (Hiraga and Kohlstedt, companion paper). Previously, and for all elements and interface types in conjunction with the volumes of the grain matrixes and the interfaces, single values for E^{α} and r_o were used for all elements and interface types to estimate the concentrations of chemical components at interfaces, and thereby predict the chemical composition of a peridotite "whole rock" (olivine–orthopyroxene–clinopyroxene) relative to the composition of a "clean rock" (Hiraga et al., 2004). As illustrated in Fig. 1, a whole rock is composed of grain matrices, plus grain and interphase boundaries, whilst a clean rock is one for which these interfaces have been removed (i.e., grain matrixes alone).

The physics behind this analysis indicates that, at least to first order, element partitioning between a grain matrix and a grain interface is the same as partitioning between a grain matrix and a silicate melt (Hiraga and Kohlstedt, companion paper). For numerous elements in olivine and clinopyroxene, values of the grain-matrix/melt partition coefficient, $KD_i^{\mathrm{GM\text{-}melt}}$, are well explained by the lattice strain model described by Eq. (2) (e.g., Beattie, 1994; Blundy and Wood, 1994). If the grain interface is taken to have a thickness of two mono-atomic lattice layers, then the interface enrichment factor, β_i, which is the ratio of $X_i^{\mathrm{interface}}$ to X_i^{GM} is approximately equal to $KD_i^{\mathrm{GM\text{-}melt}}$,

$$\beta_i \equiv X_i^{\mathrm{interface}}/X_i^{\mathrm{GM}} \approx (KD_i^{\mathrm{GM\text{-}melt}})^{-1} \quad (3)$$

(Hiraga and Kohlstedt, companion paper). Note that $KD_i^{\mathrm{GM\text{-}melt}}$ is normally obtained from measurements of the weight percent of the solute in the grains and in the melt, C_i^{GM} and C_i^{melt}, which can be approximated as $X_i \approx C_i/100$ when $X_i \ll 10^{-3}$.

In this paper, we discuss the implications of our new understanding of interface segregation to a range of topical problems in mantle geochemistry. We utilize calculated values of β_i to assess: (1) solute concentration at interfaces from the measurement of solute concentration in grain matrices, (2) the contribution of interfaces to the chemical budget of typical peridotitic mantle rocks, (3) the influence of grain size on solute concentration in grain matrixes and whole rocks, (4) grain sizes in the mantle based on solute concentration in grain matrixes, and (5) the role of interface segregation on transport of elements via interface diffusion.

2. Concentrations of elements at interfaces

Values of $KD_i^{\mathrm{GM\text{-}melt}}$ can be parameterized using the lattice strain model (e.g., Beattie, 1994; Blundy and Wood, 1994) for a wide variety of elements and phases including monovalent (e.g., K, Rb, and Cs), divalent (e.g., Sr and Ba), trivalent (e.g., Lu, Y, Nd, Ce, and La), tetravalent (e.g., U and Th), and noble gas (e.g., Ar, Ne, Kr and Xe) elements in major rock-forming minerals (i.e., olivine, orthopyroxene, clinopyroxene, plagioclase, amphibole, and garnet) (e.g., Beattie, 1994; Blundy and Wood, 1994; Bottazzi et al., 1999; van Westrenen et al., 1999; Brooker et al., 2003). Selection of appropriate values of $KD_i^{\mathrm{GM\text{-}melt}}$ must take into account the influence of major element compositions; for example, in the case of clinopyroxene, the Al_2O_3 content critically affects the value of $KD_i^{\mathrm{GM\text{-}melt}}$ (Wood and Blundy, 1997). To determine the value of β_i at the temperature at which a rock equilibrated, T^{rock}, the value of $KD_i^{\mathrm{GM\text{-}melt}}$ obtained at a certain experimental temperature, T^{ex}, must be converted to that at T^{rock}:

$$\beta_i(T^{\mathrm{rock}}) \approx \{KD_i^{\mathrm{GM\text{-}melt}}(T^{\mathrm{rock}})\}^{-1} = \{KD_i^{\mathrm{GM\text{-}melt}}(T^{\mathrm{ex}})\}^{-T^{\mathrm{ex}}/T^{\mathrm{rock}}} \quad (4)$$

Thus, published microbeam analyses of C_i^{GM} allow estimates of $C_i^{\mathrm{interface}}$ based on Eqs. (3) and (4). Estimates of T^{rock} can be derived from a range of geothermometers

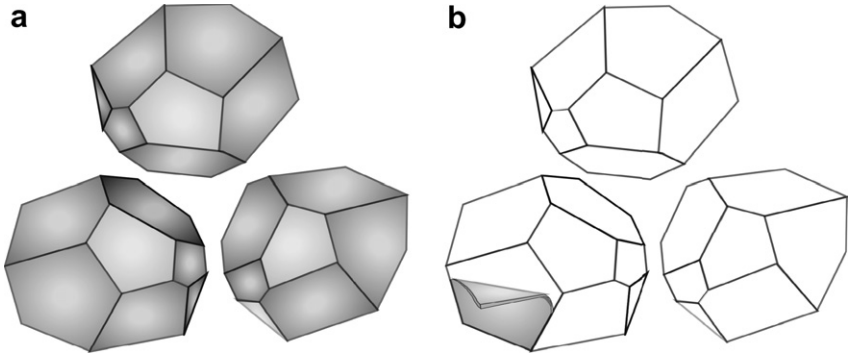

Fig. 1. Schematic illustrations of (a) a "whole" rock and (b) a "clean" rock. In (a), the grey surfaces on the grains in the whole rock represent the grain–grain interface layers. In (b), the grain interface layers have been removed or are being removed, as indicated for the lower left grain.

applicable to peridotitic xenoliths (e.g., Brey and Köhler, 1990). In theory, the value of $C_i^{\text{interface}}$ calculated from $KD_i^{\text{GM-melt}}$ of any single phase in the rock is applicable to all types of interface, and this has been verified by experimental observation (Hiraga and Kohlstedt, companion paper). We argue that Eq. (4) is widely applicable to any mineral for any element for which $KD_i^{\text{GM-melt}}$ follows the lattice strain model, since this assures that $KD_i^{\text{GM-melt}}$ is determined chiefly by strain energy in grain matrices rather than by energetics in the melt. In fact, values of $KD_i^{\text{GM-melt}}$ may vary by up to an order of magnitude owing to the effects of melt composition (e.g., Schmidt et al., 2006). Therefore, values of β_i^{whole} will contain uncertainties produced by the effect of chemical compositions on $KD_i^{\text{GM-melt}}$, though the effects of melt composition may not have strong influence on the relative order of incompatibility of elements. Empirically Eq. (4) also holds for at least some elements such as Ti for which mineral/melt partitioning behavior is not predicted easily using the lattice strain model (Hiraga and Kohlstedt, companion paper). As a first order approximation, we can use $KD_i^{\text{GM-melt}}$ to obtain β_i so long as Q_i^{seg} in Eq. (1) is influenced chiefly by solution energy in grain matrices rather than by melt energetics.

The values of β_i derived from mineral/melt partitioning in conjunction with the measurement of the concentrations of solutes in grain matrices provide a reasonable guide for estimating the concentration of various elements on grain–grain interfaces. This approach may facilitate investigation not only of the storage capacity of solutes at interfaces in a whole rock, as will be discussed in the next section, but also of the influence of grain interface segregation on interfacial properties such as grain growth (e.g., Chen and Chen, 1996; Freund et al., 2001) without direct measurement of interface chemistry, as such measurements may be experimentally challenging.

3. Whole-rock interface enrichment factor

In order to analyze the storage of elements on grain–grain interfaces in rocks consisting of more than one mineral, we introduce β_i^{whole}, which relates average concentration of i in grain matrixes, C_i^{GM}, to the concentration in the interfaces,

$$C_i^{\text{interface}} = \beta_i^{\text{whole}} \cdot C_i^{\text{GM}} \tag{5}$$

where C_i^{GM} is calculated from the mode (f) of constituent mineral (m) of the rock as

$$C_i^{\text{GM}} = \sum_m f^m \cdot C_i^{\text{GM-}m} \tag{6}$$

From Eqs. (3) and (4), Eq. (5) is rewritten as:

$$\beta_i^{\text{whole}}(T^{\text{rock}}) \approx \left\{ \sum_m f^m \cdot KD_i^{m-\text{melt}}(T^{\text{rock}}) \right\}^{-1} \tag{7}$$

This relationship is analogous to the expression commonly used in crystal-melt partitioning, $KD_i^{\text{whole-melt}}$, calculated from given values of f^m. The results of the calculation for representative elements and simple mineral modes with reported values of $KD_i^{\text{GM-melt}}$ are shown in Fig. 2. Except for the noble gases, the order of the elements listed along the horizontal axis in the figure is same as the order in a typical spider diagram (Sun and McDonough, 1989). Experimentally determined values of $KD_i^{\text{GM-melt}}$ (Kennedy et al., 1993; Beattie, 1994; Brooker et al., 2003) were used to obtain β_i^{whole} at 1373 K based on Eqs. (4) and (7) (Table 1). We selected values of $KD_i^{\text{GM-melt}}$ that are well explained by the lattice strain model with reasonable values of E^{α} and U_i^{elec} in Eq. (2), and we excluded values of $KD_i^{\text{GM-melt}}$ that are unexpectedly large, as these may be contaminated by sample preparation prior to analysis (Taura et al., 1998) or by surrounding glass and inclusions unintentionally sampled by microbeams (Beattie, 1994). Experimental data for $KD_i^{\text{ol-melt}}$ and $KD_i^{\text{opx-melt}}$ for Cs, Rb, Ne, Kr, and Xe are absent and experimental data for $KD_i^{\text{ol-melt}}$ for Ar and K may be compromised by analytical complications (Brooker et al., 1998; Taura et al., 1998). Thus, these values are taken as zero in this study. To examine the influence of mantle fertility, we calculate values of β_i^{whole} for three different peridotite compositions: a lherzolite with $(f^{\text{ol}},f^{\text{opx}},f^{\text{cpx}}) = (0.7,0.2,0.1)$, a dunite with $(f^{\text{ol}},f^{\text{opx}},f^{\text{cpx}}) = (0.9,0.09,0.01)$, and a pyroxene-rich lherzolite with $(f^{\text{ol}},f^{\text{opx}},f^{\text{cpx}}) = (0.6,0.2,0.2)$.

The predicted enrichment of incompatible elements at interfaces increases with decreasing $KD_i^{\text{GM-melt}}$ (or $KD_i^{\text{whole-melt}}$), f^{cpx}, and T^{rock}. f^{cpx} is a critical factor in determining β_i^{whole}; if f^{cpx} decreases by an order of magnitude, β_i^{whole} increases by roughly an order of magnitude. Temperature primarily affects β_i^{whole} for highly incompatible elements; this point can be appreciated by noting that

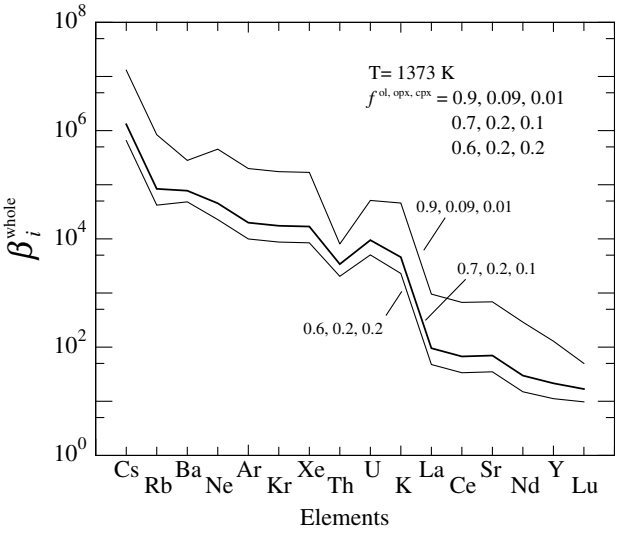

Fig. 2. Values of β^{whole} for representative incompatible elements. Values indicated by the heavy line were calculated for normal lherzolite with $(f^{\text{ol}},f^{\text{opx}},f^{\text{cpx}}) = (0.7,0.2,0.1)$. Upper and lower bounds were determined for a dunite of composition $(f^{\text{ol}},f^{\text{opx}},f^{\text{cpx}}) = (0.9,0.09,0.01)$ and for a pyroxene-rich lherzolite of composition $(f^{\text{ol}},f^{\text{opx}},f^{\text{cpx}}) = (0.6,0.2,0.2)$.

Table 1
$KD_i^{\text{GM-melt}}$ to obtain $\beta_i\,(T^{\text{rock}})$ based on Eq. (4)

	$KD_i^{\text{ol-melt}}\ (T^{\text{ex}})$	T^{ex} (K)	$KD_i^{\text{ol-melt}}\ (T^{\text{rock}})$	$KD_i^{\text{opx-melt}}\ (T^{\text{ex}})$	T^{ex}	$KD_i^{\text{opx-melt}}\ (T^{\text{rock}})$	$KD_i^{\text{cpx-melt}}\ (T^{\text{ex}})$	T^{ex}	$KD_i^{\text{cpx-melt}}\ (T^{\text{rock}})$
Cs	—	—	—	—	—	—	1.70E−05	1473	7.64E−06
Rb	—	—	—	—	—	—	2.20E−04	1473	1.19E−04
Ba	2.09E−06	1463	8.87E−07	1.70E−04	1698	2.18E−05	1.50E−04	1473	7.90E−05
Ne	—	—	—	—	—	—	3.90E−04	1473	2.20E−04
Ar	—	—	—	—	—	—	8.40E−04	1473	5.01E−04
Kr	—	—	—	—	—	—	9.50E−04	1473	5.72E−04
Xe	—	—	—	—	—	—	9.80E−04	1473	5.92E−04
Th	2.10E−04	1473	1.13E−04	1.10E−04	1698	1.27E−05	3.20E−03	1473	2.11E−03
U	1.80E−05	1473	8.12E−06	2.30E−04	1698	3.17E−05	1.50E−03	1473	9.34E−04
K	—	—	—	—	—	—	3.30E−03	1473	2.18E−03
La	3.77E−06	1463	1.66E−06	4.40E−05	1698	4.09E−06	1.22E−01	1473	1.05E−01
Ce	1.02E−05	1463	4.80E−06	1.40E−06	1698	1.71E−05	1.69E−01	1473	1.48E−01
Sr	3.94E−05	1463	2.03E−05	5.10E−04	1698	8.48E−05	1.63E−01	1473	1.43E−01
Nd	2.00E−04	1473	1.08E−04	5.20E−04	1698	8.68E−05	3.60E−01	1473	3.34E−01
Y	4.94E−03	1463	3.49E−03	9.60E−03	1698	3.20E−03	4.60E−01	1473	4.35E−01
Lu	2.00E−02	1473	1.50E−02	4.60E−02	1698	2.22E−02	4.70E−01	1473	4.45E−01

$KD_i^{\text{ol-melt}}$ at $T^{\text{ex}} = 1463$ and 1473 K are from Beattie (1994) and Kennedy et al. (1993), respectively. $KD_i^{\text{opx-melt}}(T^{ex})$ are from Kennedy et al. (1993). $KD_i^{\text{cpx-melt}}(T^{ex})$ are from Brooker et al. (2003). T^{rock} is constant as 1373 K.

$KD_{\text{Ba}}^{\text{opx-melt}}(T^{\text{ex}}) \approx 8 \times KD_{\text{Ba}}^{\text{opx-melt}}(T^{\text{rock}})$ if the difference between T^{ex} and T^{rock} is ~300 K (Table 1).

We did not take into account accessory minerals in the above calculations. Elements that dissolve into common accessory minerals may be correspondingly enriched weakly at grain interfaces, although in principle their relative concentrations can be estimated from concentrations in principal silicates (olivine and pyroxene) if their values of $KD_i^{\text{GM-melt}}$ are measured and explained by the lattice strain model. For example, the whole-rock concentration of Nb in spinel peridotites is dominated by spinel (Bodinier et al., 1996; Condie et al., 2004). Platinum group elements (PGEs) are largely excluded from lattices of the principal peridotite minerals but concentrate in accessory sulfides or metallic "nuggets" (Burton et al., 2000). The magnitude of PGE enrichments on grain interfaces is therefore uncertain, particularly considering that their oxidation state at grain interfaces is not well constrained.

4. Interface chemical component in whole rock chemistry

Based on the calculated values of β_i^{whole}, we can estimate the relative contribution of interfaces to storage of trace elements in mantle rocks. The concentration of an element in the whole rock, C_i^{whole}, is related to the average concentrations in the grain matrices, C_i^{GM}, obtained from Eq. (6) and at the grain interfaces, C_i^{inteface}, combined with the volumes of each region, V^{GM} and $V^{\text{interface}}$, through the expression

$$C_i^{\text{whole}} \approx \frac{V^{\text{GM}}}{V^{\text{interface}} + V^{\text{GM}}} \cdot C_i^{\text{GM}} + \frac{V^{\text{interface}}}{V^{\text{interface}} + V^{\text{GM}}} \cdot C_i^{\text{interface}} \tag{8}$$

The concentration of component i at the interface relative to its concentration in the whole rock is given by

$$\frac{C_i^{\text{interface}} \cdot V^{\text{interface}}}{C_i^{\text{whole}} \cdot (V^{\text{interface}} + V^{\text{GM}})} = \frac{\beta_i^{\text{whole}} \cdot V^{\text{interface}}}{V^{\text{GM}} + \beta_i^{\text{whole}} \cdot V^{\text{interface}}} \tag{9}$$

For grains shaped as tetrakaidecahedrons, the volume ratio in Eq. (9) can be expressed as

$$\frac{V^{\text{interface}}}{V^{\text{GM}}} \approx \frac{3.55}{\bar{d}} \cdot w \cdot \exp[-2.5(\ln\sigma)^2] \tag{10}$$

(Terwilliger and Chiang, 1995), where w is the grain boundary width and $\exp[-2.5(\ln\sigma)^2]$ is a correction factor that accounts for a lognormal distribution of grain size. The width of the distribution is characterized by $\ln\sigma = \ln(d/\bar{d})$, the standard deviation of normalized grain dimension, where $\bar{d}$ is the average grain size. Normally, this correction factor lies in the range 0.7–0.9. Application of Eq. (9) with values of β_i^{whole} for typical peridotites with differing mineral modes and $\bar{d}$ illustrates the effect of mineral mode and mean grain size on the interface contribution to the whole-rock chemistry (Fig. 3a and b).

The contribution of the interface component to whole-rock chemistry increases with increasing β_i^{whole} (Fig. 3). Our calculations demonstrate that whole-rock inventories of elements more compatible than K are dominated by grain-matrices. We note, however, that for K and Rb, the importance of interfaces as storage sites is not as large as previously predicted by Hiraga et al. (2004). For example, we previously concluded that effectively all of the K in a normal lherzolite is located at the interfaces, whereas our new calculations suggest that the contribution of grain–grain interfaces to the inventory of K is negligible (Fig. 3). The value of Young's modulus in Eq. (2) is smaller for monovalent elements than for divalent elements (Hiraga and Kohlstedt, companion paper); however, Hiraga et al. (2004) used a single value for Young's modulus for all elements independent of valance, which is an oversimplification.

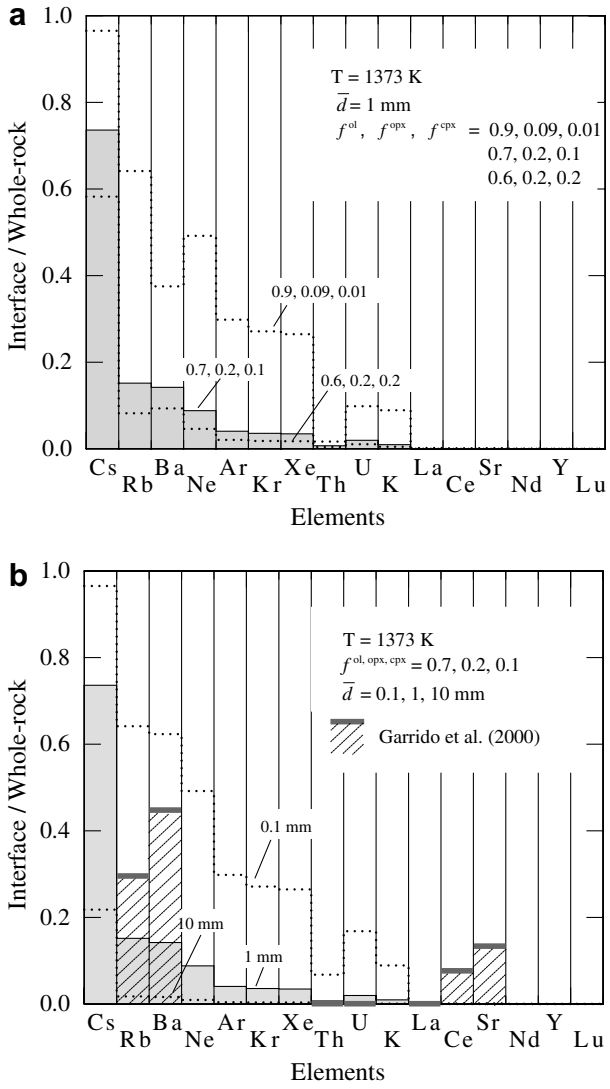

Fig. 3. Grain–grain interface contribution relative to whole-rock contribution for several elements. Calculations employ an average grain interface width, w, of 0.75 nm (Hiraga and Kohlstedt, companion paper) and a grain size correction factor, $\exp[-2.5(\ln\sigma)^2]$, of 0.8. (a) The interface contribution was calculated for aggregates with different grain sizes with a lherzolite mineral mode. (b) The interface contribution was calculated for aggregates with a fixed grain size of $\bar{d}$ = 1 mm for different rock types from dunite to pyroxene-rich lherzolite.

Numerous studies have documented whole-rock concentrations of incompatible elements that are larger than would be expected based on analyses of the matrices of mineral grains in the rock (Fig. 1). Such discrepancies require storage of significant amounts of incompatible elements in cryptic phases such as accessory minerals, glass, fluid inclusions, or interfaces (e.g., Menzies and Murthy, 1978; Ottonello, 1980; Stosch et al., 1986; Zindler and Jagoutz, 1988; Ionov et al., 1992; Garrido et al., 2000; Xu et al., 2003). In some cases the discrepancy between whole rock and clean rock concentrations has been shown to increase with increasing incompatibility (Zindler and Jagoutz, 1988; Xu et al., 2003), an observation consistent with storage of these elements at interfaces. Data for Rb, Ba, Th, U, La, Ce, and Sr from harzburgite (RC147) in Garrido et al. (2000) for which the mineral mode is $(f^{ol}, f^{opx}, f^{cpx}) = (0.72, 0.2, 0.06)$ are included in Fig. 3b. Grain size was not reported. These authors reported noticeable interface concentrations of Rb, Ba, Ce, and Sr. As shown in Fig. 3b, the concentrations estimated by Garrido et al. (2000) for Rb and perhaps Ba in harzburgite are consistent with our results for interface segregation. On the other hand, they did not observe interface components of U, Th, and La, as expected from our segregation model. In contrast, concentrations of Sr and Ce are too large to be the result of interface segregation even for a rock with a grain size of only 0.1 mm. We suggest that an unidentified intergranular phase, rather than interfaces, is responsible for storing Sr and Ce.

5. Grain size and mineral compositions

Fig. 3b illustrates that the proportion of highly incompatible elements stored at grain interfaces depends on the grain size. A corollary is that the concentrations of these elements in mineral matrices depend on grain size. Because crystal-melt partition coefficients are most commonly measured for clinopyroxene, it is useful to express C_i^{whole} for incompatible elements as

$$C_i^{whole} \approx C_i^{GM} + \beta_i^{cpx} \cdot \frac{V^{interface}}{V^{GM}} \cdot C_i^{GM\_cpx} \tag{11}$$

where C_i^{GM} is obtained from Eq. (6). It is clear from this relationship that for a rock of fixed whole-rock composition, C_i^{GM} will vary simply owing to differences in $V^{interface}/V^{GM}$, which in turn, depends on $\bar{d}$ (Eq. (10)). Thus, the proportion of a given element in a rock that is stored along interfaces is inversely proportional to grain size; consequently, the relative importance of interfaces to the inventory of incompatible elements in a rock increases as grain size decreases. Because clinopyroxene is a principle host for incompatible elements in mantle peridotite (ex., Salters and Shimizu, 1988), the approximation $C_i^{GM} \approx f^{cpx} \cdot C_i^{GM\_cpx}$ often holds for highly incompatible elements. For this case, we obtain the simple relationship between $C_i^{GM\_cpx}/C_i^{whole}$ and $\bar{d}$

$$\bar{d} = \frac{2.84 \cdot w \cdot \beta_i^{cpx}}{(C_i^{GM\_cpx}/C_i^{whole})^{-1} - f^{cpx}} \tag{12}$$

where $C_i^{GM\_cpx}/C_i^{whole}$ and $\bar{d}$ are measurable quantities. We plot this relationship for Cs, Ba and Rb for $f^{cpx} = 0.1$ in Fig. 4. For Eq. (12) to be useful, the values of β_i^{cpx} must be sufficiently large to overcome the very small values of $V^{interface}/V^{GM}$ that prevail for normal mantle grain sizes; therefore, highly incompatible elements is relatively small such for are most useful. For example, if β_i^{cpx} is as large as $\sim 10^4$ as is the case for Rb, $C_i^{GM\_cpx}/C_i^{whole}$ is not sensitive to $\bar{d}$ over the range of 1–10 mm (Fig. 4).

Eq. (12) can be used for a quick check on storage of elements on interfaces or other storage sites in rocks by

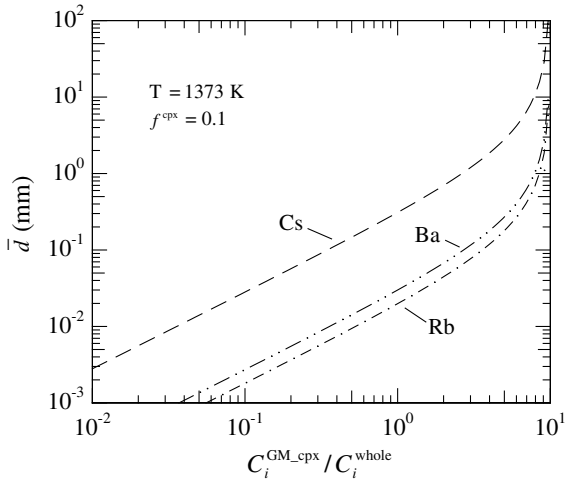

Fig. 4. Calculated relationship between mean grain size, $\bar{d}$, and the ratio between concentrations of selected elements in cpx vs. whole rock, $C_i^{GM\_cpx}/C_i^{whole}$ for $f^{cpx} = 0.1$ at $T = 1373$ K based on Eq. (12). For grain size >1 mm, only Cs shows significant variations in $C_i^{GM\_cpx}/C_i^{whole}$.

comparing the mean grain size necessary to account for inferred concentrations with the observed grain size of the rock. For the case of Rb and Ba in the harzburgite investigated by Garrido et al. (2000), we can apply Eq. (12) with $f^{cpx} = 0.06$ using measured values of $C_i^{GM\_cpx}/C_i^{whole}$ to calculate a model value of $\bar{d}$. For this rock, $C_{Rb}^{GM\_cpx}$ and C_{Rb}^{whole} are 90 and 80 ppb, while $C_{Ba}^{GM\_cpx}$ and C_{Ba}^{whole} are 180 and 210 ppb, respectively, of ~10 (Garrido et al., 2000). These suggest values of $\bar{d}$ of 20 μm, which is much smaller than the grain size of typical mantle xenoliths. Thus, it is likely that the concentrations of Rb and Ba reside also in an unidentified intergranular or included phase. Garrido et al. (2000) also concluded from their detailed chemical analyses that contributions of Rb and Ba arose not only from interfaces but also from unidentified inclusions.

Silicate glass is a likely cryptic intergranular phase that may store significant concentrations of incompatible elements. Since the interface enrichment factor is related to the crystal-melt partition coefficient, the characteristics of interface components will be similar to those resulting from an interstitial glass that may have originated from partial melting and/or melt infiltration from the host magma. If small amounts of intergranular glass are present, then calculations of $\bar{d}$ based on $C_i^{GM\_cpx}/C_i^{whole}$ will yield an unrealistically small value, but $C_i^{GM\_cpx}/C_i^{whole}$ for different incompatible elements will give similar values of $\bar{d}$. Even if an intergranular glass phase exists at a level that is not detectable by conventional observational techniques (e.g., if $f^{glass} = 0.0001$), the volume of the glass is still ~10^2 larger than the volume of the interfaces in a rock composed of grains of 1 mm diameter.

6. Grain size in earth's mantle

Grain size is a critical parameter for determining transport-related properties of the mantle such as viscosity, anelasticity, and electrical conductivity (e.g., Hirth and Kohlstedt, 1995; Jackson et al., 2002; ten Grotenhuis et al., 2004). We can predict the relationship between $C_i^{GM\_cpx}$ and $\bar{d}$ in representative melt-free mantle reservoirs such as the depleted MORB source region (Salters and Stracke, 2004) or a mantle with the composition of the bulk silicate Earth (McDonough and Sun, 1995) by substituting C_i^{mantle} for C_i^{whole} in Eq. (12) and using a constant value for f^{cpx}. Based on estimated values of C_i^{mantle} for Cs, Rb, Ba, Ne, and Ar for depleted mantle (Salters and Stracke, 2004) and using $f^{cpx} = 0.1$, the calculated relationship between $C_i^{GM\_cpx}$ and $\bar{d}$ in the mantle is presented in Fig. 5. Such relationships between grain size and concentrations of incompatible elements in mantle minerals may be helpful for estimating the grain size of the mantle.

Of all of the incompatible elements, Cs is the most promising; as shown in Fig. 5, only $C_{Cs}^{GM\_cpx}$ allows investigation the whole range of likely mantle grain sizes. As an example, if $C_{Cs}^{GM\_cpx}$ from mantle xenoliths and C_{Cs}^{whole} from depleted mantle are ~2 ppb (Bedini et al., 1997) and 1.32 ppb (Salters and Stracke, 2004), respectively, the mantle is predicted to be composed of grains ~0.5 mm in diameter (Fig. 5). Unfortunately, accurate measurements of $C_{Cs}^{GM\_cpx}$ are analytically challenging and therefore sparse. Because this highly incompatible element potentially contains important information about the physical properties of the mantle, more such analyses should be attempted.

An aggregate with a grain size of 0.1 mm has a 10 times larger capacity to store incompatible elements at grain interfaces than does an aggregate of with a grain size of 1 mm, as illustrated in Fig. 3b and amplified in Fig. 4. Thus, if C_i^{whole} and mineral mode remain constant, $C_i^{GM\_cpx}$ will decrease by an order of magnitude when $\bar{d}$ decreases by an order of magnitude. Thus, grain-size

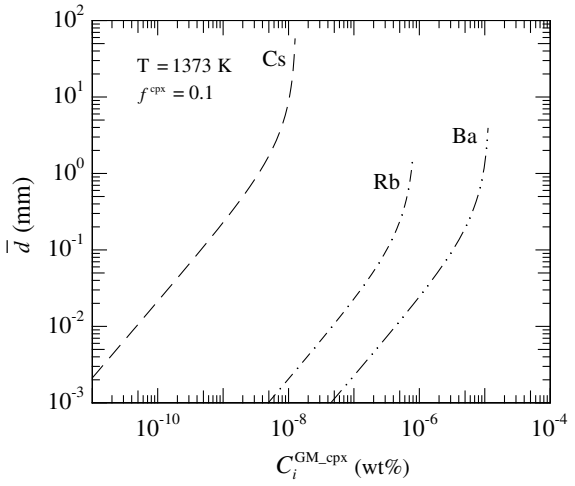

Fig. 5. Calculated relationships between solute concentrations in clinopyroxene and grain size in the mantle for $f^{cpx} = 0.1$ at $T = 1373$ K based on Eq. (12). In our calculations, $C_{Cs,Rb,Ba}^{mantle} = 1.32$, 88, and 1.2 ppm, respectively (Salters and Stracke, 2004). Note that $C_i^{GM\_cpx}$ no longer varies with $\bar{d}$ at large $\bar{d}$ and that the largest value of $\bar{d}$ for which $C_i^{GM\_cpx}/C_i^{whole}$ vs. $\bar{d}$ has a finite slope is greater for more incompatible elements.

reduction during rock deformation alone may induce a chemical potential gradient between more- and less-deformed regions in a shear zone, and this situation may conceivably lead to enhanced concentrations of incompatible elements in highly deformed mantle regions.

7. Mechanisms of mass transport

One important aspect of interface segregation is that it can influence greatly the transport properties of rocks because segregation changes the vacancy concentration and/or the atomic-bonding state at interfaces. Here we consider the simplest, geologically important case of the effect of segregation on interface diffusion. The diffusivity of element i through bulk, fluid-free polycrystalline material, D_i^{bulk}, can be expressed in terms of the diffusivities of i in the grain matrix, D_i^{GM}, and along the interface, $D_i^{\text{interface}}$, as

$$D_i^{\text{bulk}} \approx D_i^{\text{GM}} + s_i \cdot (3w/d) \cdot D_i^{\text{interface}} \tag{13}$$

where d is the grain diameter (Hart, 1957). In this equation, s_i is the segregation factor, which can be approximated as β_i. Eq. (13) states that the concentration of i at an interface is always larger by a factor of s_i than the concentration in the grain matrix at local equilibrium between the two regions. Previous studies on oxides suggest w that for diffusion is ~1 nm, similar to the thickness in metals, even though a space charge region likely exists in ionic materials (e.g., Atkinson, 1985). Such narrow widths are often attributed to distinctly different properties at the core of an interface relative to the interior of a grain. The core width should correspond to the segregation width, that is, to a thickness of about two mono-atomic layers, 0.7–0.8 nm (Hiraga and Kohlstedt, companion paper). Thus, our estimate for the width of interface segregation region is in good agreement with previously estimates of the width for interface diffusion.

Lattice diffusion is strongly affected by ionic radius in a fashion predicted from a lattice strain model (Van Orman et al., 2001). In contrast, ionic radius is not expected to influence diffusion at grain interfaces, as residence of cations residing in grain interfaces is not believed to be accompanied by significant strains, even when species have large ionic radii. Although the influence of ionic radius and electrostatic charge on interface diffusion has not been investigated systematically with experiments, we expect that the value of $D_i^{\text{interface}}$ is roughly constant for all of the incompatible elements with the same electrostatic charge, whose crystal-melt partitioning behavior is explained by the lattice strain model. This idea is supported by experimental observation that, for REE diffusing in melt, $D_{\text{REEs}}^{\text{melt}}$ is essentially independent of ionic radius (Liang et al., 2004). The ratio $D_i^{\text{interface}}/D_i^{\text{GM}}$ depends strongly on temperature, owing to differences in activation energies between grain interface diffusion and grain matrix diffusion but typical values range between 10^3 and 10^8 (Shewmon, 1989). $D_i^{\text{interface}}/D_i^{\text{GM}}$ for Mg in an olivine aggregate is $\sim 10^4$ at 1573 K (Farver et al., 1994) and $\beta_{\text{Mg}} \approx 1$ (Hiraga and Kohlstedt, 2007). Since Mg is essentially a strain free element in the olivine lattice, the lattice strain model predicts that $D_i^{\text{interface}}/D_i^{\text{GM}}$ assumes a minimum value for Mg and increases with increasing lattice strain in the matrix; thus $D_i^{\text{interface}}/D_i^{\text{GM}}$ is expected to be $>10^4$ for most of diffusing incompatible elements. If $D_i^{\text{interface}}/D_i^{\text{GM}} = 10^4$, interface diffusion and lattice diffusion contribute equally to the transport of element i through a rock when $s_i \cdot (3w/d) \times 10^4 = 1$ as can be seen in Eq. (13). Accordingly, if the range of $s_i \cdot (3w/d) \times 10^4 > 1$ for a particular ion, then interface diffusion should be the dominant mechanism of mass transport through a rock. Calculated values for $s_i \cdot (3w/d) \times 10^4$ for various incompatible elements in olivine and clinopyroxene aggregates composed of 1 mm grains at a temperature of 1573 K, representative conditions for the asthenosphere, are illustrated in Fig. 6. In an olivine-rich rock, $s_i \cdot (3w/d) \times 10^4 > 1$ for most incompatible elements. As mantle rocks are composed chiefly of olivine, the plots in Fig. 6 show that most incompatible elements with enrichment factors are larger than that of Lu will predominantly be transported through a fluid-free mantle via interface diffusion. Interface diffusion may also dominate for pyroxene rich rocks, but only for highly incompatible elements (i.e., those more incompatible than La).

Thus, interface diffusion may be of great importance for numerous transport phenomena in the mantle, such as transport of noble gases (e.g., He and Ar) and siderophile elements (e.g., Pt and Os) (Watson, 2002), and homogenization of isotopes in a heterogeneous mantle (e.g., Hofmann and Hart, 1978; Kogiso et al., 2004).

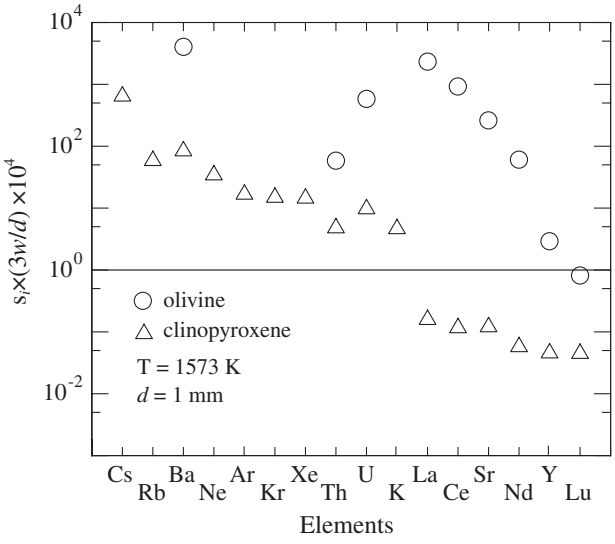

Fig. 6. Calculated values for the interface diffusion parameter $s_i \cdot (3w/d) \times 10^4$ in Eq. (13) for olivine and clinopyroxene aggregates at 1573 K. A reference line at $s_i \cdot (3w/d) \times 10^4 = 1$ is inserted to indicate the condition at which grain interface diffusion and grain matrix diffusion contribute equally for the case $D_i^{\text{interface}}/D_i^{\text{GM}} = 10^4$.

8. Water at interfaces?

An important question bearing on the physical and chemical properties of the mantle is the extent to which H is concentrated on grain interfaces. Detection of H at grain boundaries is experimentally very challenging (e.g., Reichart et al., 2004); however, it has been suggested that hydrogen concentrates on olivine grain boundaries and influences grain boundary properties (e.g., Kohn, 1996; De Leeuw et al., 2000; Mei and Kohlstedt, 2000; Jung and Karato, 2001). It is unlikely that mineral/melt partitioning of H can be parameterized easily using the lattice strain theory, in part because it is difficult to define an ionic radius for H and in part because of the complexity of H substitutions in silicate lattices (Libowitzky and Beran, 2004). However, $KD_{\mathrm{H}}^{\mathrm{GM\text{-}melt}}$ appears to be controlled mostly by energetics in the grain matrix, which is supported by the observation that $KD_{\mathrm{H}}^{\mathrm{GM\text{-}melt}}$ lies between the values of $KD_{i}^{\mathrm{GM\text{-}melt}}$ for La and Ce (Dixon et al., 1988; Michael, 1988, 1995; Danyushevsky et al., 2000; Aubaud et al., 2004; Hauri et al., 2006). Since values of $KD_{\mathrm{H}}^{\mathrm{GM\text{-}melt}}$ for La and Ce follow the lattice strain model, $\beta_{\mathrm{H}}^{\mathrm{ol}}$ and $\beta_{\mathrm{H}}^{\mathrm{whole}}$ are likely to be $1/KD_{\mathrm{H}}^{\mathrm{ol\text{-}melt}} \approx 10^{3}$ and $1/KD_{\mathrm{H}}^{\mathrm{whole\text{-}melt}} \approx 10^{2}$, respectively (Fig. 2). These values should be valid only at relatively low pressures; at high pressures the storage capacity of H in grain matrices becomes very large (e.g., Kohlstedt et al., 1996), and consequently $\beta_{\mathrm{H}}^{\mathrm{whole}}$ is probably reduced, as is also expected to be true for $KD_{\mathrm{H}}^{\mathrm{whole\text{-}melt}}$ (Asimow et al., 2004). Otherwise the concentration of H at the interface would exceed the saturation level of a region two mono-atomic layers thick. If $\beta_{\mathrm{H}}^{\mathrm{whole}} \approx 10^{2}$, then interfaces do not play a significant role in storing water in the mantle (Fig. 3), but such enrichments may be large enough to change the physical properties of grain–grain interfaces, either by influencing atomic bonding and/or vacancy concentrations (Mei and Kohlstedt, 2000).

Above, we introduced a method for calculating the concentration of elements on grain interfaces, and presented some applications using examples from simple mantle peridotite. However, the analysis explored here is not limited to a single rock type, and should be applicable to a wide range of lithologies, including garnet-bearing mantle rocks or crustal rocks, so long as values of $KD_{i}^{\mathrm{GM\text{-}melt}}$ (or $KD_{i}^{\mathrm{whole\text{-}melt}}$) are constrained for the rock-forming minerals.

Acknowledgments

We acknowledge discussions with E.B. Watson, C.A. Lee, A.C. Withers, and C. Aubaud. T.H. was partially supported by a Gibson Fellowship through the Department of Geology and Geophysics, University of Minnesota. The research was funded through NSF Grant EAR-0409719.

Associate editor: Martin A. Menzies

References

Atkinson, A., 1985. Grain boundary diffusion—structural effects and mechanisms. *J. Physique* **46**, C4 379–C4 391.

Asimow, P.D., Dixon, J.E., Langmuir, C.H., 2004. A hydrous melting and fractionation model for mid-ocean ridge basalts: application to the Mid-Atlantic Ridge near the Azores. *Geochem. Geophys. Geosyst.* **5**, Q01E16. doi:10.1029/2003GC00056.

Aubaud, C., Pineau, F., Jambon, A., Javoy, M., 2004. Kinetic disequilibrium of C, He, Ar and carbon isotopes during degassing of mid-ocean ridge basalts. *Earth Planet. Sci. Lett.* **222**, 391–406.

Beattie, P., 1994. Systematics and energetics of trace-element partitioning between olivine and silicate melts: implications for the nature of mineral/melt partitioning. *Chem. Geol.* **117**, 57–71.

Bedini, R.M., Bodinier, J.–L., Dautria, J.–M., Morten, L., 1997. Evolution of LILE-enriched small melt fractions in the lithospheric mantle: a case study from the East African Rift. *Earth Planet. Sci. Lett.* **153**, 67–83.

Blundy, J., Wood, B., 1994. Prediction of crystal-melt partition coefficients from elastic moduli. *Nature* **372**, 452–454.

Bodinier, J.–L., Merlet, C., Bedini, R.M., Simien, F., Remaidi, M., Garrido, C.J., 1996. Distribution of niobium, tantalum and other highly incompatible trace elements in the lithospheric mantle: the spinel paradox. *Geochim. Cosmochim. Acta* **60**, 545–550.

Bottazzi, P., Tiepolo, M., Vannucci, R., Zanetti, A., Brumm, R., Foley, S.F., Oberti, R., 1999. Distinct site preferences for heavy and light REE in amphibole and the prediction of $^{\mathrm{Amph/L}}D_{\mathrm{REE}}$. *Contrib. Mineral. Petrol.* **137**, 36–45.

Brey, G.P., Köhler, T., 1990. Geothermobarometry in four-phase lherzolite II. New thermobarometers, and practical assessment of existing thermobarometers. *J. Petrol.* **31**, 1353–1378.

Brooker, R.A., Wartho, J.–A., Caroll, M.R., Kelley, S.P., Draper, D.S., 1998. Preliminary UVLAMP determinations of argon partition coefficient for olivine and clinopyroxene grown from silicate melts. *Chem. Geol.* **147**, 185–200.

Brooker, R.A., Du, Z., Blundy, J.D., Kelley, S.P., Allan, N.L., Wood, B.J., Chamorro, E.M., Wartho, J.–A., Purton, J.A., 2003. The 'zero charge' partitioning behaviour of noble gases during mantle melting. *Nature* **423**, 738–741.

Burton, K.W., Schiano, P., Birck, J.-L., Allègre, C.J., Rehkämper, M., Halliday, A.N., Dawson, J.B., 2000. The distribution and behaviour of rhenium and osmium amongst mantle minerals and the age of the lithospheric mantle beneath Tanzania. *Earth Planet. Sci. Lett.* **183**, 93–106.

Chen, P.-L., Chen, I.-W., 1996. Grain growth in CeO_2: dopant effects, defect mechanism, and solute drag. *J. Am. Ceram. Soc.* **79**, 1793–1800.

Condie, K.C., Cox, J., O'Reilly, S.Y., Griffin, W.L., Kerrich, R., 2004. Distribution of high field strength and rare earth elements in mantle and lower crustal xenoliths from Southwestern United States: the role of grain-boundary phases. *Geochim. Cosmochim. Acta* **68**, 3919–3942.

Danyushevsky, L., Eggins, S.M., Falloon, T.J., Christie, D.M., 2000. H_2O abundance in depleted to moderately enriched mid-ocean ridge magmas: Part 1: incompatible behaviour, implications for mantle storage, and origin of regional variations. *J. Petrol.* **41**, 1329–1364.

De Leeuw, N.H., Parker, S.C., Catlow, R.A., Price, D., 2000. Proton-containing defects at forsterite {0 1 0} tilt grain boundaries and stepped surface. *Am. Mineral.* **85**, 1143–1154.

Dixon, J.E., Stopler, E.M., Delaney, J.R., 1988. Infrared spectroscopic measurements of CO_2 and H_2O in Juan de Fuca Ridge basaltic glasses. *Earth Planet. Sci. Lett.* **90**, 87–104.

Farver, J.R., Yund, R.A., Rubie, D.C., 1994. Magnesium grain boundary diffusion in forsterite aggregates at 1000–1300 °C and 0.1 MPa to 10 GPa. *J. Geophys. Res.* **99**, 19809–19819.

Freund, D., Rybacki, E., Dresen, G., 2001. Effect of impurities on grain growth in synthetic calcite aggregates. *Phys. Chem. Minerals* **28**, 737–745.

Garrido, C.J., Bodinier, J.-L., Alard, O., 2000. Incompatible trace elements partitioning and residence in anhydrous spinel peridotites and websterites from the Rhonda orogenic peridotite. *Earth Planet. Sci. Lett.* **181**, 341–358.

Hart, E.W., 1957. On the role of dislocations in bulk diffusion. *Acta Metal.* **5**, 597.

Hauri, E.H., Gaetani, G.A., Green, T.H., 2006. Partitioning of water during melting of the Earth's upper mantle at H_2O-undersaturated conditions. *Earth Planet. Sci. Lett.* **248**, 715–734.

Hiraga, T., Anderson, I.M., Kohlstedt, D.L., 2004. Grain boundaries as reservoirs of incompatible elements in the Earth's mantle. *Nature* **427**, 699–703.

Hiraga, T., Kohlstedt, D.L., 2007. Equilibrium interface segregation in the diopside–forsterite system I: Analytical techniques, thermodynamics, and segregation characteristics. *Geochim. Cosmochim. Acta* **71**, 1266–1280.

Hirth, G., Kohlstedt, D.L., 1995. Experimental constraints on the dynamics of the partially molten upper mantle: deformation in the diffusion creep regime. *J. Geophys. Res.* **100**, 1981–2001.

Hofmann, A.W., Hart, S.R., 1978. An assessment of local and regional isotopic equilibrium in the mantle. *Earth Planet. Sci. Lett.* **38**, 44–62.

Ionov, D.A., Kramm, U., Stosch, H.-G., 1992. Evolution of the upper mantle beneath the southern Baikal rift zone: an Sr–Nd isotope study of xenoliths from the Bartoy volcanoes. *Contrib. Mineral. Petrol.* **111**, 235–247.

Jackson, I., Fitz Gerald, J.D., Faul, U.H., Tan, B.H., 2002. Grain-size-sensitive seismic wave attenuation in polycrystalline olivine. *J. Geophys. Res.* **107**, 2360. doi:10.1029/2001JB00122.

Jung, H., Karato, S-I., 2001. Effects of water on dynamically recrystallized grain-size of olivine. *J. Struct. Geol.* **23**, 1337–1344.

Kennedy, A.K., Lofgren, G.E., Wasserburg, G.J., 1993. An experimental study of trace element partitioning between olivine, orthopyroxene and melt in chondrules: equilibrium values and kinetic effect. *Earth Planet. Sci. Lett.* **115**, 177–195.

Kogiso, T., Hirschmann, M.M., Reiners, P.W., 2004. Length scale of mantle heterogeneities and their relationship to ocean island basalt geochemistry. *Geochim. Cosmochim. Acta* **68**, 345–360.

Kohlstedt, D.L., Keppler, H., Rubie, D.C., 1996. Solubility of water in the α, β and γ phases of $(Mg,Fe)_2SiO_4$. *Contrib. Mineral. Petrol.* **6**, 345–357.

Kohn, S.C., 1996. Solubility of H_2O in nominally anhydrous mantle minerals using ^1H MAS NMR. *Am. Mineral.* **81**, 1523–1526.

Liang, Y., Cherniak, D.J., Morgan, Z.T., Hess, P.C., 2004. Eu^{2+} and REE^{3+} diffusion in enstatite, diopside, anorthite, and a silicate melt: a database for understanding kinetic fractionation of REE in the lunar mantle and crust. *Lunar and Planetary Science Conference* **XXXV**, #1894.

Libowitzky, E., Beran, A., 2004. IR spectroscopic characterization of hydrous species in minerals. In: Beran, A., Libowitzky, E., (Eds.), *Spectroscopic Methods in Mineralogy*, EMU Notes in Mineralogy, Eotvos University Press, vol. 6, pp. 227–279.

McDonough, W.F., Sun, S.-S., 1995. The composition of the Earth. *Chem. Geol.* **120**, 223–253.

McLean, D., 1957. *Grain Boundaries in Metals*. Clarendon Press, Oxford.

Mei, S., Kohlstedt, D.L., 2000. Influence of water on plastic deformation of olivine aggregates: 1. diffusion creep regime. *J. Geophys. Res.* **105**, 21457–21469.

Menzies, M.M., Murthy, V.R., 1978. Strontium isotope geochemistry of alpine tectonite lherzolites: data compatible with a mantle origin. *Earth Planet. Sci. Lett.* **38**, 346–354.

Michael, P.J., 1988. The concentration, behaviour and storage of H_2O in the suboceanic upper mantle: implications for mantle metasomatism. *Geochim. Cosmochim. Acta* **52**, 555–566.

Michael, P.J., 1995. Regionally distinctive sources of depleted MORB: evidence from trace elements and H_2O. *Earth Planet. Sci. Lett.* **131**, 301–320.

Reichart, P., Datzman, G., Hauptner, A., Hertenberger, R., Wild, C., Dollinger, G., 2004. Three-dimensional hydrogen microscopy in diamond. *Science* **306**, 1537–1540.

Ottonello, G., 1980. Rare earth abundances and distribution in some spinel peridotite xenoliths from Assab (Ethiopia). *Geochim. Cosmochim. Acta* **44**, 1885–1901.

Salters, V.J.M., Shimizu, N., 1988. World-wide occurrences of HFSe-depleted mantle. *Geochim. Cosmochim. Acta* **52**, 2177–2182.

Salters, V.J.M., Stracke, A., 2004. Compositions of the depleted mantle. *Geochem. Geophys. Geosyst.* **5** (5), Q05004. doi:10.1029/2003GC00059.

Schmidt, M.W., Connolly, J.A.D., Günther, D., Bogaerts, M., 2006. Element partitioning: the role of melt structure and composition. *Science* **312**, 1646–1650.

Shewmon, P., 1989. *Diffusion in Solids*. The Minerals, Metals and Materials Society, Pennsylvania.

Stosch, H.-G., Lugmair, G.W., Kovalenko, V.I., 1986. Spinel peridotite xenoliths from the Tariat Depression, Mongolia. II: geochemistry and Nd and Sr isotopic composition and their implications for the evolution of the subcontinental lithosphere. *Geochim. Cosmochim. Acta* **50**, 2601–2614.

Sun, S.-S., McDonough, W.F., 1989. Chemical and isotopic systematics of oceanic basalts: implications for mantle composition and processes. In: Saunders, A.D., Norry, M.J. (Eds.), *Magmatism in the Ocean Basins*, 42. Geological Society Special Publication, London, pp. 313–345.

Taura, H., Yurimoto, H., Kurita, K., Sueno, S., 1998. Pressure dependence on partition coefficient for trace elements between olivine and the coexisting melts. *Phys. Chem. Minerals* **25**, 469–484.

Terwilliger, C.D., Chiang, Y.-M., 1995. Size-dependent solute segregation and total solubility in ultrafine polycrystals: Ca in TiO_2. *Acta Metall. Mater.* **43**, 319–328.

ten Grotenhuis, S.M., Drury, M.R., Peach, C.J., Spiers, C.J., 2004. Electrical properties of fine-grained olivine: evidence for grain boundary transport. *J. Geophys. Res.* **109**, B06203. doi:10.1029/2003JB00279.

Van Orman, J.A., Grove, T.L., Shimizu, N., 2001. Rare earth element diffusion in diopside: influence of temperature, pressure, and ionic radius, and an elastic model for diffusion in silicates. *Contrib. Mineral. Petrol.* **141**, 687–703.

van Westrenen, W., Blundy, J.D., Wood, B.J., 1999. Crystal-chemical controls on trace element partitioning between garnet and anhydrous silicate melt. *Am. Mineral.* **84**, 838–847.

Watson, E.B., 2002. Mobility of siderophile elements in grain boundaries of periclase and periclase/olivine aggregates. *Eos: Trans. Am. Geophys. Union* **83**, Spring Meet. Suppl., Abstract V52B-03.

Wood, B.J., Blundy, J.D., 1997. A predictive model for rare earth element partitioning between clinopyroxene and anhydrous silicate melt. *Contrib. Mineral. Petrol.* **129**, 166–181.

Xu, X., O'Reilly, S.Y., Griffin, W.L., Zhou, X., 2003. Enrichment of upper mantle peridotite: petrological, trace element and isotopic evidence in xenoliths from SE China. *Chem. Geol.* **198**, 163–188.

Zindler, A., Jagoutz, E., 1988. Mantle cryptology. *Geochim. Cosmochim. Acta* **52**, 319–333.